THE JOURNAL OF PHYSICAL CHEMISTRY B
A JOURNAL OF THE AMERICAN CHEMICAL SOCIETY

pubs.acs.org/JPCB

Article

Pushing Camera-Based Single-Molecule Kinetic Measurements to the Frame Acquisition Limit with Stroboscopic smFRET

David A. Nicholson and David J. Nesbitt*

Cite This: *J. Phys. Chem. B* 2021, 125, 6080−6089

Read Online

ACCESS | Metrics & More | Article Recommendations | Supporting Information

ABSTRACT: Single-molecule fluorescence resonance energy transfer (smFRET) experiments permit detailed examination of microscopic dynamics. However, kinetic rate constants determined by smFRET are susceptible to systematic underestimation when the rate constants are comparable to the data acquisition rate. We demonstrate how such systematic errors in camera-based total internal reflection fluorescence microscopy experiments can be greatly reduced by using stroboscopic illumination/detection, allowing accurate rate constant determination up to the data sampling rate and yielding an order of magnitude increase in the dynamic range. Implementation of these stroboscopic smFRET ideas is straightforward, and the stroboscopically obtained data are compatible with multiple trajectory analysis methods, including dwell-time analysis and hidden Markov modeling. Such stroboscopic methods therefore offer a remarkably simple yet valuable addition to the smFRET toolkit, requiring only relatively modest modification to the normal data collection and analysis procedures.

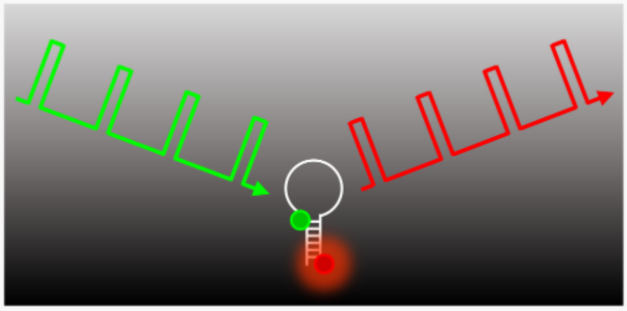

1. INTRODUCTION

Single-molecule microscopy is a powerful tool for examining kinetic systems at otherwise inaccessible levels of detail. From the folding of biopolymers,[1,2] to single enzyme catalysis,[3,4] to single DNA replication[5] and transcription,[6] both *in vitro* and *in vivo*,[7−9] as well as nonbiological applications,[10,11] the ability to probe at the sub-ensemble level clarifies underlying mechanisms in ways that are impossible in bulk studies. Especially powerful in the field of biophysics has been the use of single-molecule fluorescence resonance energy transfer (smFRET),[12−14] in which spatial motion on biologically relevant length scales (1−10 nm) can be converted into a colorimetric ratio, the FRET efficiency (E_{FRET}). By monitoring the time-dependence of E_{FRET} for surface-tethered molecules, structural rearrangements can be observed in real time. Stochastic state-to-state hopping in E_{FRET} trajectories can then be analyzed to extract dynamical information, for example, the number of thermally accessible states and the rate constants for interconversion between those states.

smFRET experiments perform well when rate constants are slow compared to the data acquisition rate, but rate constants that are comparable to or exceed the sampling rate pose additional challenges. In particular, these faster rate constants are susceptible to systematic underestimation, with bias becoming significant even for as little as $k \geq 10\%$ of the sampling rate.[15] This systematic error/bias arises from well-known distortion of the FRET distributions by "camera averaging" or "camera blurring."[16,17] Similar to "motional blur" in conventional still photography, the multiple FRET states become temporally averaged over (*i.e.*, "blur") with increasingly larger exposure times, introducing artifactual density in the FRET histograms and intercalation between the true FRET values. These blurred FRET values present problems for accurate kinetic analysis of the data and can even incorrectly suggest the existence of additional, nonphysical states.[15]

The simplest way to avoid such bias is obviously to increase the acquisition rate, which, for camera-based detection include options such as cropping the field of view or performing on-chip pixel binning. To push hardware limitations even further, Tang *et al.* have achieved increased effective frame rates through use of sparse imaging and a galvo-mirror.[18] However, each of these options requires sacrificing some multiplexing capacity of the experiment, which is indeed a primary benefit of widefield methods over non-multiplexed detection such as scanning confocal microscopy.[19,20] Instead, it would be more desirable to mitigate camera averaging effects while still maintaining the highest possible parallel throughput of data.

More sophisticated smFRET data analysis methods incorporate such camera averaging effects directly. For instance, much work has been put into modeling the resulting

Received: February 3, 2021
Revised: May 4, 2021
Published: June 7, 2021

https://doi.org/10.1021/acs.jpcb.1c01036
J. Phys. Chem. B 2021, 125, 6080−6089

distorted distributions,[21] as in probability distribution analysis (PDA).[22−24] A more agnostic approach is taken by Chen *et al.*[25] in which the experimentally determined (underestimated) rate constants are least squares compared with those derived from simulated data subject to the same camera averaging artifact. The parameters of the kinetic model are then iteratively varied until the simulated results match the experiment. While effective, this simulate−compare−iterate approach requires accurate modeling of the experimental system and is therefore prone to introducing additional systematic errors.

In the present work, we propose a relatively simple experimental solution based on stroboscopic illumination to eliminate camera averaging effects. Stroboscopes have been used before in single-molecule microscopy, especially in single-particle tracking, where a flashing light source can reduce diffusional blurring to increase accuracy in position determination.[26−28] Our interest in the strobe is not to reduce *motional* blur but rather to reduce *temporal* blur. Our development builds on the work of Farooq and Hohlbein,[29] who used stroboscopic imaging to mimic the fluorescence burst data from confocal diffusing studies and then analyzed the FRET histogram using PDA. Here, we show that stroboscopic data can be analyzed as trajectories, which has the benefit of utilizing the full information content of the smFRET data and permits rate constant determination up to the data acquisition rate. Under typical smFRET experimental conditions, this translates into roughly an order of magnitude enhancement in data collection bandwidth for trajectory-based analysis, free from systematic underestimation of rate constants.

2. METHODOLOGY

2.1. Theory of Single-Molecule Kinetics. The kinetic systems studied in single-molecule experiments can be abstractly represented as a finite set of discrete states $\{S_i\}$ which undergo state-to-state transitions governed by first-order kinetics. Specifically, the state transitions are considered Poisson processes, with k_{ij} as the unimolecular rate constants for state S_j converting to state S_i. The rate of change of the population in state S_i is the sum of the total loss rate and the total production rate

$$\frac{\mathrm{d}}{\mathrm{d}t}S_i = -\sum_{j\neq i} k_{ji}S_i + \sum_{j\neq i} k_{ij}S_j \tag{1}$$

One may compactly express the total rate of change of all states in matrix-vector form by forming the state vector $\mathbf{S} = \{S_1, S_2, ...\}$ and the rate matrix $\mathbf{K}$ (with off-diagonal elements $K_{ij} = k_{ij}$ and on-diagonal elements $K_{ii} = -\sum_{j\neq i} k_{ji}$) which satisfy the master equation

$$\frac{\mathrm{d}}{\mathrm{d}t}\mathbf{S} = \mathbf{K}\mathbf{S} \tag{2}$$

From eq 1, it is clear that the sum of any column of $\mathbf{K}$ vanishes, which is equivalent to the conservation of molecular number. The solution to this system of differential equations is

$$\mathbf{S}(t) = \mathrm{e}^{\mathbf{K}t}\mathbf{S}_0 = \mathbf{T}(t)\mathbf{S}_0 \tag{3}$$

where $\mathbf{S}_0$ is the initial state distribution at $t = 0$ and $\mathbf{T}(t)$ is the time evolution operator. In eq 3, the matrix exponential operator is evaluated by Taylor series expansion as $\mathrm{e}^{\mathbf{K}t} = (\mathbf{I} + \mathbf{K}t + (\mathbf{K}t)^2/2 + (\mathbf{K}t)^3/(3!) + ...)$, where $\mathbf{K}t$ simply multiplies each element of $\mathbf{K}$ by t and $\mathbf{I}$ is the identity matrix.

To connect this formalism, which is based on ensemble chemical kinetics, to the dynamics of single-molecule systems, $\mathbf{T}(t)$ is interpreted as the matrix of transition probabilities at lag time t. Specifically, the matrix element $T_{ji}(t - t')$ is the probability that the system will be in state j at time t after being in state i a time t' earlier. Note that this does not specify which path the system took to reach the final state j. Indeed, $T_{ji}(t)$ includes all possible trajectories the system could take to go from i to j (*e.g.*, $i\rightarrow j$, $i\rightarrow k\rightarrow j$, $i\rightarrow j\rightarrow i\rightarrow j$). For stroboscopic experiments, this has important implications, discussed below, in which the experimentalist is "blind" for some fraction of the observation time window.

2.2. Photon-By-Photon Trajectory Simulation. Single-molecule trajectories are simulated using a photon-by-photon approach, similar to that of Szabo and Gopich.[30] This is carried out in two steps: (i) simulation of the state of the molecular system as a function of time $S(t)$ followed by (ii) simulation of the fluorescently emitted and detected photons. First, the initial state S_0 (*e.g.*, 0 or 1 for array element $i = 1, n$) for the molecule is randomly selected from an equilibrium probability vector $\mathbf{p}_{eq}$, corresponding to the unique eigenvector of the rate matrix $\mathbf{K}$ with an eigenvalue of zero. Time is then iteratively forward-propagated by randomly choosing a dwell time for the current state i, which is exponentially distributed with a time constant associated with the total loss rate from that state, that is, $-1/K_{ii}$. The next state index is then randomly selected, with a probability weighted by the branching ratio into the selected target state j, $P(i \rightarrow j) = K_{ji}/\sum_{j\neq i} K_{ji}$, with this exponential time propagation continued until the desired total simulation time is achieved.

After the state trajectory $S(t)$ is generated, a sequence of individual photon detection events is produced. Similar to the case for state transitions, photon detection is assumed to be a Poisson process, which is accurate for a fluorophore excitation rate small compared to the fluorescence rate $I_{fluor} = 1/\tau_{fluor}$, where τ_{fluor} is the fluorescence lifetime. In this limit, single photons will arrive exponentially distributed in time as determined by the photon detection rate k_{photon}. In general, k_{photon} can be a function of the conformational state of the molecule, for example, due to a FRET pair with different quantum yields. However, many FRET dye pairs, in particular, the Cy3−Cy5 pair used in the present experiments, have very similar quantum yields, which motivates treating k_{photon} as constant, though deviations could be easily incorporated into the kinetic model. The color of the emitted photon is probabilistically distributed based on the conformation (*i.e.*, FRET state) of the molecule at the time of the excitation event. Specifically, the photon is labeled as an "acceptor" with probability E_i or a "donor" with probability $(1 - E_i)$, where E_i is the FRET efficiency of the molecule in state i. As with the state trajectories, the process of exponential time-jumping and assignment of photon color is continued until the full desired simulation window is achieved. Lastly, photons are binned at the frame time Δt_{frame} to generate donor and acceptor average intensities as a function of time, $D(t)$ and $A(t)$, respectively. Note that all noise considered in the modeled data arises exclusively from quantum fluctuations ("shot noise") in the photon counting process. While other sources such as dark count noise and read noise[31] are also present in camera-based smFRET, the experimental conditions we are interested in place the system well within the limit where shot noise

https://doi.org/10.1021/acs.jpcb.1c01036
J. Phys. Chem. B 2021, 125, 6080−6089

dominates over all other sources of noise. This simulation method can be extended to include background donor and acceptor average count rates (B_D and B_A); however, the effect of adding background photons can be equivalently achieved by (1) shifting the FRET efficiencies and (2) increasing the relative noise by decreasing the photon detection rate, and therefore for simplicity, we have set the background intensities to zero in these studies. The MATLAB code for performing these trajectory simulations and kinetic analysis (see below) will be made available upon request.

2.3. Single-Molecule Microscopy. smFRET experiments are performed on a DNA hairpin by total internal reflection fluorescence (TIRF) microscopy, as described previously.[32] Briefly, a 7 bp DNA hairpin[33] with a 40-adenine loop is biotinylated at the 3′ end and attached to a glass surface *via* streptavidin−biotin binding.[34] The hairpin is labeled with Cy3 and Cy5 for FRET-based conformational detection. The DNA construct is imaged in 50 mM HEPES buffer (pH = 7.6) with 70 mM total monovalent cations (K^+ and Na^+) and a PCA−PCD−TROLOX oxygen-scavenging and triplet quenching cocktail for enhanced fluorophore photostability.[35,36] A diode-driven Nd:YAG laser illuminates the surface-attached DNA construct in a through-objective TIRF configuration.[37] Fluorescence is separated by a dichroic mirror into donor (Cy3) and acceptor (Cy5) channels, which are each focused onto one-half of an intensified charge-coupled device (ICCD) array. To achieve stroboscopic (gated) illumination, the diode light output is modulated by a variable duty cycle square-wave current profile generated in LabVIEW (NI, Austin, TX), which also triggers the ICCD to initiate frame acquisition. Movies are analyzed using homebuilt software programmed in LabWindows/CVI to extract single-molecule trajectories. Particles are located by brightness thresholding and then sorted into donors and acceptors and paired based on relative location. Finally, integration inside a 2-pixel radius around particle centers then generates donor and acceptor intensity trajectories, $D(t)$ and $A(t)$.

2.4. Single-Molecule Trajectory Analysis. *2.4.1. Dwell-Time Analysis.* In the simplest mode of analysis, time-dependent FRET trajectories are computed from the binned donor $[D(t)]$ and acceptor $[A(t)]$ intensities by $\mathrm{FRET}(t) = A(t)/[A(t) + D(t)]$, where we assume any corrections for differential donor *versus* acceptor quantum yields to be negligible. Simple two-state thresholding at the arithmetic mean of low and high FRET values is applied to the FRET trajectories to determine the state function, $S(t)$, with the temporal duration between threshold crossings yielding a histogram of dwell times $N(\Delta t_{\mathrm{dwell}})$. This dwell-time histogram is then re-expressed as the "survival probability" $P(\Delta t_{\mathrm{dwell}})$ for a given conformational state lasting longer than $\Delta t_{\mathrm{dwell}}$, with single exponential fits for folded state dwell times (Δt_{fold}) yielding the unfolding rate constant k_{unfold} (and *vice versa*).

2.4.2. Hidden Markov Modeling. As a second analysis scheme, Hidden Markov modeling (HMM) is performed by computing the likelihood function (L) of observing an experimental FRET trajectory given a set of model parameters and then finding the parameter values that maximize L. For a FRET trajectory E_n of temporal length $N\Delta t_{\mathrm{frame}}$, the scalar probability L is computed as

$$L = \mathbf{1}^{\mathrm{T}} * \left[\prod_{n=2}^{N} \mathbf{O}(E_n) * e^{\mathbf{K} * \Delta t_{\mathrm{frame}}} \right] * \mathbf{O}(E_1) * \mathbf{p}_{\mathrm{eq}} \tag{4}$$

This equation is read right to left, where $\mathbf{p}_{\mathrm{eq}}$ is the equilibrium probability vector, $\mathbf{O}(E_n)$ is the diagonal matrix of observation probabilities for the nth observed FRET value, $\mathbf{K}$ is the rate matrix, $\Delta t_{\mathrm{frame}}$ is the time between frames, and $\mathbf{1}^{\mathrm{T}}$ is the row vector $(1, 1, ...)$ of length equal to the number of states in the system. Diagonal elements of the observation matrix (O_{ii}) are the probabilities of observing a FRET value in the state i, which we model as Gaussian variables, that is, $O_{ii}(E) \propto \exp[-(E - E_i)^2/2\sigma i^2)$ with center E_i and width σ_i. Gradient ascent is used to determine the set of parameters (k_{ij}, E_i, σ_i) which maximize L, where L is periodically renormalized to avoid instabilities due to numerical underflow.[38] Note that this probability is maximized by optimization of the rate matrix elements K_{ij} rather than the transition probabilities T_{ij}, which avoids inaccuracies and instabilities due to computation of the matrix logarithm $\mathbf{K} = \ln(\mathbf{T})/\Delta t_{\mathrm{frame}}$.

2.4.3. Time-Correlation Function Analysis. In the third kinetic analysis approach, time-correlation functions (TCFs) are computed for the four possible combinations of donor and acceptor intensities: $\langle D(t)D(t+\tau)\rangle$, $\langle D(t)A(t+\tau)\rangle$, $\langle A(t)D(t+\tau)\rangle$, and $\langle A(t)A(t+\tau)\rangle$. For example, $\langle D(t)A(t+\tau)\rangle$ reflects the donor−acceptor cross-correlation function given by

$$D(t)A(t+\tau) = \sum_{\mathrm{i}} P_{\mathrm{i}} D_{\mathrm{i}} \left(\sum_{\mathrm{f}} P_{\mathrm{i}\to\mathrm{f}}(\tau) A_{\mathrm{f}} \right) \tag{5}$$

In eq 5, P_i is the equilibrium probability of initial state i, D_i the average donor intensity in state i, $P_{i\to f}(\tau)$ is the transition probability from i to f in lag time τ, A_f is the average acceptor intensity in the final state f, and the summation is over all initial and final states. Additional contributions to the TCF from fast dynamics (*e.g.*, fluorophore blinking) are not included as the time resolution of these CCD measurements is typically in the 10s of the milliseconds domain, far longer than the time scales of such photophysical behavior in Cy3 and Cy5[36] (in effect, these contributions are statically incorporated into A_i and D_i). We may therefore generalize to any combination of donor and acceptor TCFs by writing eq 5 in matrix form as

$$\frac{C_1(t)C_2(t+\tau)}{I^2} = \mathbf{1}^{\mathrm{T}} * \mathbf{E}(C_2) * \mathbf{T}(\tau) * \mathbf{E}(C_1) * \mathbf{p}_{\mathrm{eq}} \tag{6}$$

where the channel C_k is now labeled by either donor D or acceptor A, $\mathbf{p}_{\mathrm{eq}}$ is the equilibrium probability vector, $\mathbf{E}(C_k)$ is a diagonal matrix whose diagonal elements are FRET efficiencies in each conformational state (*i.e.*, E_i if $C_k = A$ or $(1 - E_i)$ for $C_k = D$), $\mathbf{T}(\tau)$ is the transition probability matrix at lag time τ equal to $\exp(\mathbf{K}\tau)$, and $\mathbf{1}^{\mathrm{T}}$ is the row vector $(1, 1, ...)$ of length equal to the number of states in the system. Here, we have normalized the TCFs by the square of the total intensity $[I^2 = (D_i + A_i)^2]$, which for comparable quantum yields is only weakly dependent on the system state, and have exploited the simple definition of the FRET efficiency as $E_i = A_i/(A_i + D_i)$. The four TCFs are evaluated at nonnegative integer multiples of the frame time $\Delta t_{\mathrm{frame}}$ and simultaneously fit to eq 6 by minimizing the sum of the squares of the residuals in MATLAB.

3. SIMULATION RESULTS

3.1. Fast Rate Constants are Systematically Underestimated in smFRET Experiments. To establish the effects of bin time on smFRET-derived rate constants, we begin by analyzing our simulation ("synthetic") single-molecule fluorescence trajectories. The primary benefit of such an approach

https://doi.org/10.1021/acs.jpcb.1c01036
J. Phys. Chem. B 2021, 125, 6080−6089

is that the actual simulation parameters are known precisely, allowing the computation of absolute and asymmetrical errors. Additionally, use of the simulations permits rapid testing of these kinetic analysis methods over the full parameter space, including modifying parameters not typically under experimental control, such as rate constants. There are numerous protocols for modeling single-molecule trajectories;[30,31] we opted for a photon-by-photon approach, in which both state-to-state transitions and photon detection events are treated as continuous-time processes, with the simulated photon arrivals binned by time/color into frames (Δt_{frame}) to generate discrete-time fluorescence trajectories of a typical CCD-based smFRET experiment. In doing so, we make no assumptions as to how photons are distributed per time bin, nor are requirements imposed that a molecule remain in a given state for the entire bin. Since camera averaging is a result of mapping from continuous-time to discrete-time processes, this photon-by-photon approach is ideal for capturing and modeling such artifacts.

We introduce our model for camera averaging by considering the two-state system in Figure 1a, which interconverts between two well-resolved FRET states (E_{low} = 0.2, E_{high} = 0.8), with forward rate k_F = 20.0 s^{-1} and reverse rate k_R = 10.0 s^{-1}, and achieves a total fluorescence signal-to-noise ratio (SNR = I/σ_I, where σ_I is the standard deviation in the brightness I) of 10:1 (100 photons per frame). Simulated trajectories of 200 s length are binned with Δt_{frame} from 5 ms to 150 ms and are subjected to conventional dwell-time analysis[39] to determine the apparent rate constants plotted in Figure 1b. Both k_F and k_R are accurately determined at short bin times but are systematically underestimated as these rate constants become comparable to the frame rate (k_{frame} = 1/Δt_{frame}). As Figure 1b clearly highlights, the magnitude of systematic rate constant errors smoothly increases in transition to the fast rate constant regime (k_F,$k_R \approx k_{frame}$).

The source of this systematic rate constant underestimation is due to errors in the transformation between continuous-time dynamics and discrete-time measurements. The true state of a system is a continuous function of time (Figure 2a), which is converted into a sequence of discrete frames by temporal binning (Figure 2b). The ideal, noiseless FRET value equals the time-weighted average of all FRET values visited in Δt_{frame}, with frames consisting of a single state i exhibiting a constant E_i FRET value. Conversely, frames for which the system has traversed multiple states in Δt_{frame} present an average FRET value contaminated by each of the individual FRET values. As a result of this FRET averaging,[16,17] accurately assigning which state or combination of states the system occupies in each frame becomes difficult. However, FRET averaging is not problematic, since long as frames with more than one state occur infrequently. This will be true if the sampling frame rate is much faster than the rates of interconversion between states ($-K_{ii} \ll k_{frame}$). Indeed, the measured rate constants for the synthetic data agree well with the extracted rate constants for sufficiently fast (k_{frame} > 10 k_F, k_R) frame rates (Figure 1b). However, when the frame rate is within an order of magnitude of k_F or k_R, the increased probability of a frame containing multiple states results in many frames with incorrect state assignments. Since the theoretical basis of most analyses of single-molecule trajectories assumes single-state occupancy per

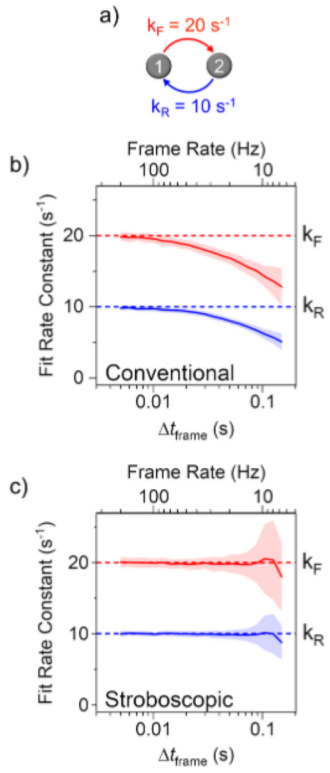

Figure 1. Systematic underestimation of rate constants in a model system. (a) Markov schematic of a two-state system governed by rates k_F = 20.0 s^{-1} and k_R = 10.0 s^{-1}. Simulated trajectories are analyzed by dwell-time analysis to extract rate constants as a function of camera frame length for (b) continuous illumination and (c) stroboscopic illumination (20% duty cycle). Shaded regions represent $\pm 1\sigma$ uncertainty bands. Simulation conditions: 2000 s, E_{low} = 0.2, E_{high} = 0.8, and 100 photons per frame (SNR = 10), repeated for each Δt_{frame} until standard error of the mean $\sigma_{SEM} = \sigma/\sqrt{N}$ reached 0.5%.

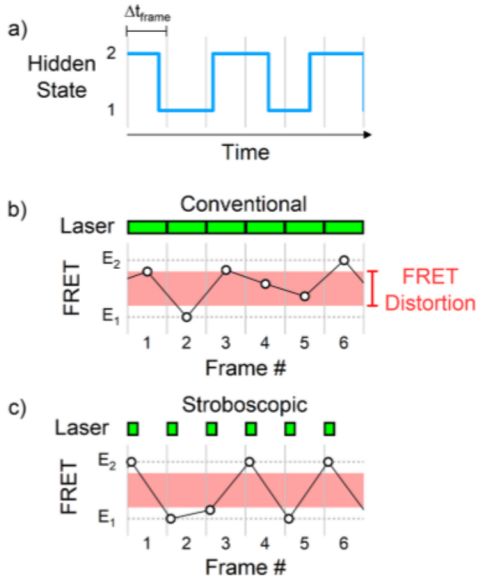

Figure 2. Mapping of continuous-time dynamics onto discrete-time results in blurred FRET states. (a) Sample true (hidden) state trajectory over six camera frames. (b,c) Ideal, noiseless FRET values averaged over time window during which laser is on (green blocks) for (b) continuous illumination and (c) stroboscopic illumination.

https://doi.org/10.1021/acs.jpcb.1c01036
J. Phys. Chem. B 2021, 125, 6080−6089

frame, faster rate constants lead to a greater fraction of frames that are unmodeled. In addition to making accurate state assignment difficult, fast rate constants and/or slow frame rates result in fundamentally "missed dynamics." Short excursions to a state lasting less than one frame will only result in slightly altered FRET efficiency, which will be misinterpreted as if no transition had occurred at all. The number of threshold-crossing transitions in a given smFRET trajectory will be lower than expected, resulting again in systematic underestimation of the rate constants. We note that simply discarding the shortest dwell times (<1−2 frames), as is sometimes performed to account for spurious short dwell times,[39] is insufficient to correct the underestimation of rate constants (Supporting Information, Figure S1).

3.2. Stroboscopic Illumination Eliminates Rate Constant Underestimation. To help resolve this issue, we propose an extremely simple solution which uses stroboscopic illumination to effectively address both FRET-averaging and missed dynamics as fundamental causes of rate constant underestimation. In a stroboscopic smFRET experiment, the excitation time window is compacted into a small fraction of the full frame. This reduction in the duty cycle can be accomplished in a variety of ways, including modulating the excitation laser current, gating the CCD detection, or simply using an analog optical chopper wheel. Reducing the time per frame that the molecule is interrogated increases the probability that the molecule occupies only one state for the duration of the observation pulse (Figure 2c). For example, in a two-state system with $k_{\text{frame}} \approx k_F, k_R$, the probability of remaining in a single state for an entire frame is on average only $1/e = 37\%$. The same system with a 10% duty cycle strobe will have a survival probability $\exp(-k\Delta t_{\text{strobe}}) = 90\%$, which makes state assignment more accurate and lowers the probability of both FRET averaging and missed dynamics.

The experimental "cost" of implementing stroboscopic methods is that one is blind to the molecular-state behavior during the window duration when the illumination is off. We address this with the second component of the proposed technique, which involves analytical correction to the measured rate constants accounting for missed transitions. This correction incurs negligible computational cost and in fact becomes exact in the limit of vanishing strobe pulse width. In the interest of space, we briefly motivate and describe how to calculate the correction, with a complete derivation to be found in the Appendix. The first correction is specific to dwell-time analysis, in which each state's survival function is fit to an exponential distribution to obtain an apparent rate constant k_i^{app}. For fast frame rates, k_i^{app} is approximately the total rate constant for leaving state i, but more generally k_i^{app} is related to the single-frame self-transition probability T_{ii} by

$$T_{ii} = e^{-k_i^{\text{app}} * \Delta t_{\text{frame}}} \tag{7}$$

In our corrected treatment, one first computes the diagonal elements T_{ii} of the transition probability matrix $\mathbf{T}$, from which the full matrix $\mathbf{T}$ can be constructed. This is particularly trivial for a two-state system, as each of the columns of $\mathbf{T}$ must sum to 1. For more complex systems, empirical branching ratios are required, as addressed in the Appendix. The second step in the correction applies to any method that measures the transition probability matrix $\mathbf{T}$ (*e.g.*, hidden Markov Modeling), in which the rate constant matrix $\mathbf{K}$ is determined from $\mathbf{T}$ by computing the matrix logarithm

$$\mathbf{K} = \frac{\ln(\mathbf{T})}{\Delta t_{\text{frame}}} \tag{8}$$

which yields the desired corrected rate constants as matrix elements K_{ij}. Note that the common approximation $\mathbf{K} = (1/\Delta t_{\text{frame}})(\mathbf{T} - \mathbf{I})$ is only accurate in the slow rate constant regime $(-K_{ii}\Delta t_{\text{frame}} \ll 1)$, with the full matrix logarithm required when measuring rate constants comparable to the data acquisition rate. Fortunately, there are a number of computationally efficient algorithms available for performing this matrix logarithm.[40,41]

Combining stroboscopic illumination with the matrix logarithm correction abrogates the systematic underestimation of rate constants in our simulated smFRET data, as seen in Figure 1c. The forward and reverse rate constants determined by dwell-time analysis under a 20% duty cycle strobe recapitulate the simulated values quite well and are independent of the choice of bin time. Neither the strobe nor analytical correction alone is sufficient to completely remove the systematic error, with only the combination correctly addressing the underlying complications of state-averaging and missed dynamics. Additional random (non-systematic) errors are also observed at large frame times (shaded uncertainty bands in Figure 1c; note that these uncertainties are standard deviations σ, whereas the standard error of the mean $\sigma_{\text{SEM}} = \sigma/\sqrt{N}$ can be decreased to arbitrary precision by repeating the measurement N times and averaging). In this regime, the average dwell time is shorter than a single frame, and the dwell-time distributions cover only a few frames in time, which increases uncertainty in fitting. Said differently, the information content of the trajectory diminishes as frame-to-frame correlations become sufficiently weak. This loss of correlation generates an upper limit on the rate constants measurable with this combination of techniques for a given frame time, as will be empirically verified in Section 3.4.

3.3. Camera Averaging Artifacts Cannot Be Resolved by Modified Experimental Conditions. One is tempted to think that it is possible to reduce or eliminate such underestimation of rate constants by the control of experimental parameters (*e.g.*, laser intensity). However, this is not the case. To explicitly address this possibility, we have performed data simulations over a wide variety of "experimental" conditions, as summarized in Figure 3a−e and which reveal no impact on rate constant deviations. By way of example, the results shown in Figure 3a represent simulations under identical conditions as in Figure 1 but with a 1:1 rather than 2:1 ratio of forward/reverse rate constants. Notice that the rate constants bias becomes significant (*i.e.*, >5%, as indicated by the yellow-banded region) at $k\Delta t_{\text{frame}} \geq 0.2$, in agreement with previous observations.[15] As a second example, we can increase the signal-to-noise ratio (SNR) by 4× (Figure 3b), which improves the accuracy of state identification but has little effect on avoiding rate constant underestimation error. This is because binning-induced broadening of FRET values is fundamentally not related to shot noise on the photon stream but rather on the state-transition dynamics. Third, we can increase the total duration of the FRET trajectories (*e.g.*, by obtaining data from more molecules), which reduces statistical noise in the measured rate constants but once again has little effect on the systematic bias (Figure 3c). As a fourth example, we might hope to modify the two-state FRET efficiencies to be better resolved (Figure 3d), which could be experimentally

https://doi.org/10.1021/acs.jpcb.1c01036
J. Phys. Chem. B 2021, 125, 6080−6089

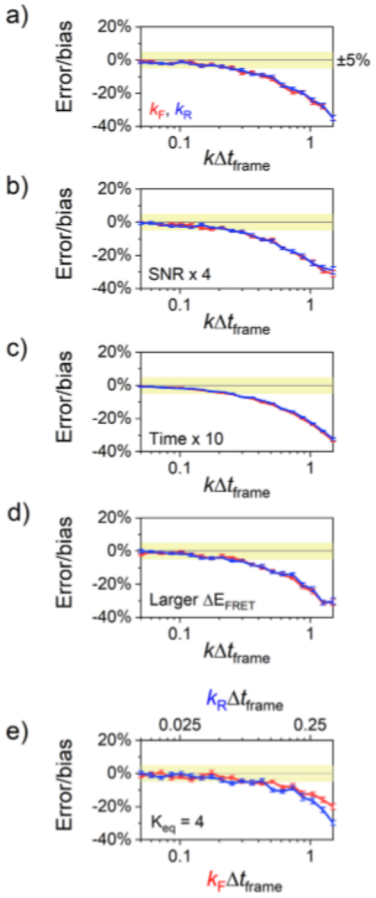

Figure 3. Camera averaging artifacts are robust to experimental parameters. (a) Bias as percent error in rate constants for simulated two-state systems with equal forward and backward rate constants. Simulation conditions: 2000 s, E_{low} = 0.2, E_{high} = 0.8, $k_F = k_R$, and 100 photons per frame (SNR = 10), repeated 24 times to determine uncertainties (standard error of the mean). For reference, the yellow region demarks a ±5% bias. (b–e) Same as (a) but simulation conditions are modified as follows: (b) 4× greater SNR ratio, (c) 10× more simulated time, (d) increased FRET separation from $\Delta E_{FRET} = E_{high} - E_{low}$ = 0.6 to 1.0, and (e) increased equilibrium constant from K_{eq} = 1 to 4 by decreasing k_R.

achieved by redesigning the single-molecule construct to optimize placement of the fluorophores. However, an increase in ΔE_{FRET} from 0.6 to 1.0 leaves the rate constant underestimation errors remarkably similar. Finally, increasing the equilibrium constant from K_{eq} = 1 to 4 (in Figure 3e by reducing the reverse rate k_R by 4×) leads to only small differences in the errors for k_F and k_R, with the average magnitude of the bias unchanged. In summary, systematic underestimation of fast rate constants by camera averaging and missing dynamics proves to be remarkably insensitive to the choice of parameters potentially under experimental control.

3.4. Optimal Excitation Duty Cycle and Maximum Measurable Rate Constants. We have shown that introducing a low duty cycle (*i.e.*, stroboscopic) light source can help eliminate binning-related artifacts in smFRET studies, but this obviously can result in loss of signal, SNR, and reduction in performance. To compensate for the loss of signal, the experimentalist may wish to increase laser power, but this also has obvious limits due to photophysics (*e.g.*, photobleaching, triplet-state formation) and nonlinearity in fluorophore brightness when the time interval between photoexcitation events approaches the fluorescence lifetime. Therefore, it is a useful exercise to identify the largest duty cycle that still reduces systematic errors to acceptable levels. To determine this optimal strobe duty cycle, we have simulated smFRET data over a range of duty cycles, rate constants, and frame acquisition rates (Figure 4). For a fixed

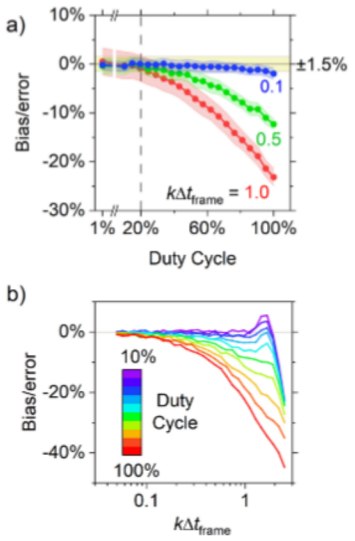

Figure 4. Determining the optimal strobe duty cycle. (a) Rate constant bias as a function of duty cycle, for fixed $k\Delta t_{frame}$ (1.0, red; 0.5, green; 0.1, blue). Duty cycle of 100% corresponds to no strobe. Shaded bands indicate uncertainties ($\pm 1\sigma$). Bias band of ±1.5% highlighted in yellow and recommended duty cycle (<20%) indicated by the vertical dashed line. (b) Rate constant bias at fixed duty cycles. The quality of results decreases for $k\Delta t_{frame} > 1$. Simulation conditions: 8000 s, $k_F = k_R$, E_{low} = 0.2, E_{high} = 0.8, and 100 photons per frame (SNR = 10). For 2D heatmaps of bias and uncertainty for combinations of duty cycle and framerate, see Supporting Information, Figure S2.

$k\Delta t_{frame}$ (Figure 4a), a decrease in strobe duty cycle monotonically reduces systematic error. However, under real-world experimental conditions, single-molecule rate constants might have typical statistical uncertainties of several percent or larger; hence, reduction of these systematic errors to <3% is usually unwarranted. For rate constants equal to the frame rate ($k\Delta t_{frame}$ = 1), we observe in Figure 4a that a strobe duty cycle of 10–20% already has reduced systematic error in the extracted rates to <3%. Obviously for rate constants lower than the frame rate ($k\Delta t_{frame}$ < 1), one achieves this 3% error limit target even more quickly with a reduction in duty cycle. Alternatively summarized, below a 10% duty cycle, one is discarding signal for little gain in extracted rate constant accuracy.

The corresponding upper limit in the measured rate constants is determined by the data acquisition rate. Trajectory-based analyses of rate constants rely on frame-to-frame correlations, and these methods fail when kinetic relaxation occurs on the time scale of the frame rate. Indeed, this mode of failure is readily observable in the shaded uncertainty regions in the right-hand side of Figure 1c, for which even the stroboscopic data produce results with high levels of statistical noise when the rate constants exceed ≈1.5 k_{frame}. Simply stated, this is due to low information content per

https://doi.org/10.1021/acs.jpcb.1c01036
J. Phys. Chem. B 2021, 125, 6080−6089

frame when the system decorrelation is fast. In this limit, individual data points in the FRET trajectory therefore become uncorrelated and can provide only non-dynamical information (*e.g.*, equilibrium constants). This same behavior can also be noted in Figure 4b, where even for low-duty-cycle data acquisition, the quality of results decays quickly at $k_F, k_R > k_{frame}$. In summary, stroboscopic smFRET methods can help rescue rate constants up to the frame rate, but faster rate constants require alternative approaches, such as stroboscopic probability distribution analysis discussed below.[29]

4. EXPERIMENTAL TESTS

To demonstrate that the above results and predictions based on simulated data are experimentally valid, we have performed a series of smFRET experiments measuring kinetic rate constants with and without stroboscopic illumination (Figures 5 and 6). Specifically, we choose to examine a very simple

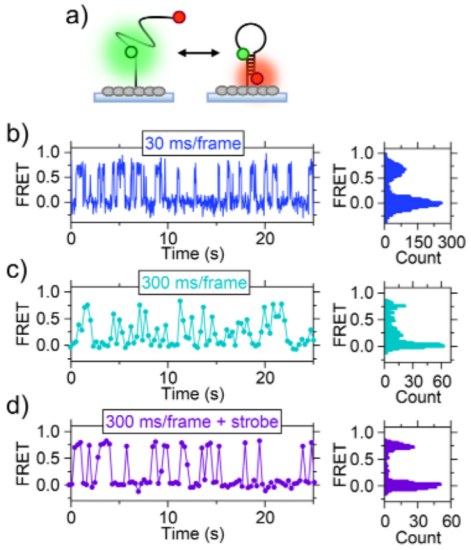

Figure 5. Experimental evaluation of stroboscopic smFRET. (a) Cartoon depiction of two-state DNA hairpin investigated in these studies. (b) Sample smFRET trajectory (left) taken at a fast frame rate (30 ms frame^{-1}) compared to underlying dynamics. FRET histogram (right) exhibits two well-resolved peaks. (c) Same as (b), but for a slow frame rate (300 ms frame^{-1}). Many frames contain intermediate FRET values due to camera averaging. (d) Same as (c) but using stroboscopic illumination at 20% duty cycle.

single-molecule construct consisting of a DNA hairpin with a 7 base-pair stem and 40-adenine loop which we have studied previously (Figure 5a).[33] This construct exhibits well-behaved two-state single-exponential kinetics (with $k_{fold} = 1.2\ s^{-1}$, $k_{unfold} = 2.2\ s^{-1}$) and therefore represents a useful model system with which to test these stroboscopic analysis methods. The data collection is performed on a TIRF[37] microscope apparatus with charge-coupled device (CCD) camera detection, and the incident laser power is increased or decreased to maintain a constant SNR ≈ 7 at all acquisition rates. As shown in Figure 5b at fast frame rates, smFRET trajectories under continuous illumination exhibit switching between two states, with the integrated FRET histogram (right panel) clearly depicting two distinct FRET peaks. On the other hand, continuous illumination at a 10× slower frame rate (Figure 5c) yields a notably smeared smFRET histogram, with spurious density

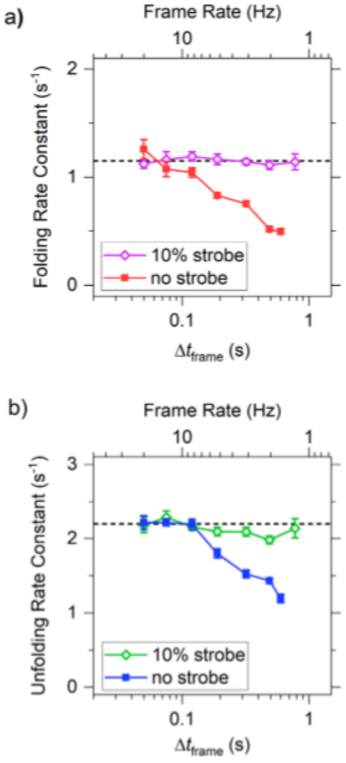

Figure 6. Experimental validation of stroboscopic method by measuring DNA hairpin folding dynamics over a range of camera frame rates. (a) Folding rate constants. Without stroboscopic illumination (red), the measured folding rate constant is a function of frame rate. Application of a 10% duty cycle strobe (purple) removes the dependence. (b) Same as (a), but for the unfolding rate constants. Each data point represents an analysis of 2000−3000 observed dwell times from ∼50 molecules. Error bars are standard errors of the mean as determined by bootstrapping.

appearing between the two FRET states. By way of contrast, however, the use of a 10% duty cycle strobe at this same slow frame rate (Figure 5d) removes camera averaging artifacts from the FRET histogram (far right), therefore restoring distinct two-state behavior.

Furthermore, the rate constants from the smFRET trajectories were measured by dwell-time analysis over a range of data acquisition bandwidths (40 to 1.3 Hz, Figure 6). Without stroboscopic illumination, the extracted rate constants exhibit the behavior characteristic of our simulated results, that is, with the measured rate constants (filled squares) systematically dependent on frame rate and underestimated with increasing Δt_{frame}. The inclusion of a 10% duty cycle strobe (open diamonds) completely removes this dependence on frame rate, in agreement with our simulations. Indeed, the kinetic measurements remain faithful even up to $k\Delta t_{frame} = 1.7$, which agrees with our upper limit of $k\Delta t_{frame} \approx 1.5$ predicted above.

5. DISCUSSION

smFRET has proven itself to be an invaluable technique for measuring the detailed dynamics of biological processes.[13,14] However, this work demonstrates that rate constants determined in such smFRET experiments can be prone to systematic underestimation, particularly when the conformational state-to-state transition rates are comparable to the data

https://doi.org/10.1021/acs.jpcb.1c01036
J. Phys. Chem. B 2021, 125, 6080−6089

acquisition rate ($k\Delta t_{frame} \gtrsim 0.1$). Herein, we have presented an extremely simple "stroboscopic" method for eliminating such "camera averaging" artifacts by restricting fluorescence collection to a reduced but contiguous portion of each time bin, for instance, by gating the excitation-light source. We have demonstrated that the use of stroboscopic data collection, together with a simple mathematical correction, can accurately recover rate constant information up to the data acquisition rate, validating these methods on both synthetic (Figure 1) and experimental (Figure 6) data. As a result, stroboscopic smFRET methods in principle extend the upper limit of measurable rate constants by up to an order of magnitude over that of conventional smFRET without resorting to reducing the instrument throughput by cropping the field of view to increase frame rates.

We can extend the use of stroboscopic smFRET one step further. The issue of systematic rate constant underestimation due to time binning is ubiquitous and generates similar constraints for more sophisticated smFRET trajectory analysis methods such as hidden HMM[39,42−44] and TCF fitting.[45,46] Consequently, each of these and other analysis methods might also benefit from stroboscopic data collection. To explore this in more detail, we have analyzed simulated smFRET trajectories using each of the three methods: (i) dwell-time analysis, (ii) HMM, and (iii) TCF fitting, under both continuous and stroboscopic illumination conditions (Figure 7). As clearly evident in Figure 7b,c (filled symbols), neither HMM nor TCF fitting escapes this fundamental issue of underestimating fast rate constants. This is quite simply because both methods make the assumption, as in dwell-time analysis, that the system occupies a single state throughout each observation point. This assumption becomes more nearly correct when fractional duty cycle "stroboscopic" illumination is applied, with all methods accurately estimating the rate constant for a 10% duty cycle excitation (Figure 7, open symbols). Consequently, the data in Figure 7 demonstrate that stroboscopic smFRET improves the accuracy of rate constant determination by other analysis methods besides dwell-time analysis. In addition, the use of HMM enables an especially facile extension of the stroboscopic method to systems of more than two states, as demonstrated in Supporting Information, Figure S3.

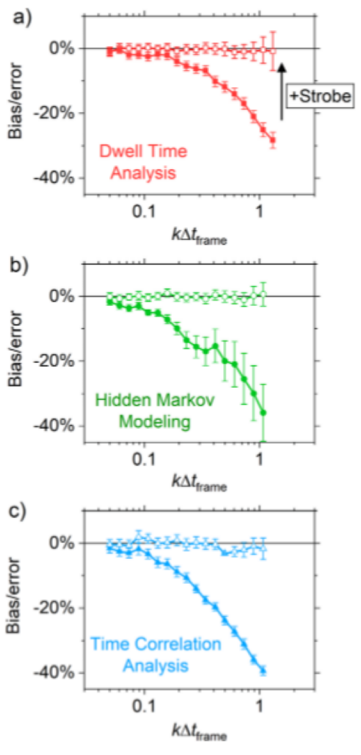

Figure 7. Systematic underestimation of rate constants is a shared feature of multiple smFRET analysis methods. Simulated conditions are the same as in Figure 3a. (a) Dwell-time analysis. (b) HMM. (c) TCF fitting. Each analysis is performed on data simulated under full-frame illumination (solid symbols) as well as 25% duty cycle stroboscopic illumination (open symbols). Error bars are $\pm 1\sigma$.

Stroboscopic smFRET requires greater laser power than conventional smFRET to obtain the same signal level, which can potentially exacerbate issues of fluorophore saturation and photobleaching. To examine this effect, we collected stroboscopic data with a 20% duty cycle at 100 frames per second (Supporting Information, Figure S4), which is approximately the full-frame capture rate of current CCD technology. Working at our maximum available laser fluence (≈50 mW over a 20 μm diameter TIR spot), we observed a 50% reduction in SNR compared to that of non-stroboscopic data at the same conditions (SNR = 3 *vs* 6; Figure S4a). Despite the loss of SNR, the quality of the data is sufficient for dwell-time analysis, and the extracted rate constants are equivalent to those obtained without stroboscopic illumination (Figure S4b, c). These results show that, with the help of oxygen removal[35] and triplet quenching,[36] fluorophore photophysics does not impede stroboscopic smFRET operation at acquisition rates up to 100 Hz.

This article is an extension of the work of Farooq and Hohlbein[29] who first demonstrated the use of stroboscopic smFRET to measure fast rate constants. However, instead of analyzing stroboscopic data by trajectory-based analyses, as in these studies, Farooq and Hohlbein used PDA.[22−24] In PDA, data points are binned into a FRET histogram, which is then fit to a model that includes kinetic parameters. Therefore, PDA treats each observed FRET value as an independent measurement. In contrast, trajectory-based analysis (*e.g.*, dwell-time analysis, HMM, TCF fitting) makes use of the correlation between data points, which has the potential advantage of utilizing a greater portion of the information content of the data. Therefore, intuitively, the trajectory-based method presented in this paper should yield rate constants with smaller uncertainties than those determined by PDA. Indeed, when simulated data are analyzed by both PDA and dwell-time analysis, the results from dwell-time analysis have ≈50% smaller uncertainties (Supporting Information, Figure S5). This reduction in uncertainty may make the present method more attractive to some smFRET researchers, especially those who already rely on trajectory-based analysis and do not wish to switch to PDA, and entirely different form of analysis. However, as shown by Farooq and Hohlbein, the combination of stroboscopic smFRET and PDA has in principle access to faster dynamics than stroboscopic trajectory analysis, as stroboscopic PDA is limited by the exposure time rather than the frame duration. Due to this combination of factors, we consider the trajectory-based approach and the PDA-based approach to be complementary methods for analyzing stroboscopic smFRET data.

We emphasize that stroboscopic smFRET is quite straightforward to incorporate into any existing smFRET

https://doi.org/10.1021/acs.jpcb.1c01036
J. Phys. Chem. B 2021, 125, 6080−6089

experiment, with stroboscopic illumination implementable at a relatively low cost. Furthermore, stroboscopic data does not require adopting new analysis methods, as it is fully compatible with conventional dwell-time, HMM, and TCF analyses. Therefore, any smFRET laboratory can readily incorporate stroboscopic methods while largely maintaining the current experimental arrangement and analysis. In the interest of completeness and kinetic rigor, we recommend reporting frame acquisition rates along with published rate constants, as well as closely monitoring the ratio of smFRET-measured rate constants to this acquisition rate. If any rate constants exceed 10−20% of the frame rate, then FRET averaging is a significant concern, for which application of stroboscopic methods offers a reduction in rate constant systematic errors down to <3% level. Finally, while this paper has focused on using smFRET to determine conformational dynamics, such a stroboscopic approach should also be extendable to any experimental method based on a fluorescence measurement of discrete-state sampling, such as transitions between diffusional states in single-molecule diffusion studies[7] or binding processes studied by protein-induced fluorescence enhancement (PIFE).[47]

6. CONCLUSIONS

We have developed, tested, and presented a stroboscopic solution to the underestimation of rate constants in time-binned smFRET experiments. Our wok demonstrates that kinetic rate constants are significantly *underestimated* when comparable to the sampling rate, with >5% systematic errors arising when rate constants are faster than 10% of the frame rate. These deviations cannot be avoided by modifying experimental parameters such as light intensity or trajectory duration. The core cause of the artifact is the mapping of continuous-time dynamics onto a discrete-time domain of binned data, resulting in blurring of FRET states and missed dynamics. These fundamental issues can be addressed through the combined use of (i) stroboscopic illumination and (ii) analytic mathematical correction to the rate constants. Stroboscopic smFRET is thereby capable of measuring rate constants up to at least the data acquisition rate, which for a 5% threshold of measurement accuracy amounts to a tenfold increase in dynamic range. This allows one to measure single-molecule rate constants up to the frame acquisition rate limit without compromising any other multiplexing capacity of the measurement.

■ ASSOCIATED CONTENT

Supporting Information

The Supporting Information is available free of charge at https://pubs.acs.org/doi/10.1021/acs.jpcb.1c01036.

Appendix deriving correction to rate constants determined by dwell-time analysis, description of PDA implementation, dwell-time analysis with short dwells removed, 2D heatmaps of bias and uncertainty versus duty cycle and $k\Delta t_{frame}$, HMM of three-state system, 10 ms/frame experimental results, and performance comparison of PDA and dwell-time analysis. The MATLAB code utilized to perform such trajectory simulations and kinetic analysis will be made available upon reasonable request of the corresponding author (PDF)

■ AUTHOR INFORMATION

Corresponding Author

David J. Nesbitt − *National Institute of Standards and Technology and University of Colorado, JILA, Boulder, Colorado 80309, United States; Department of Chemistry and Department of Physics, University of Colorado, Boulder, Colorado 80309, United States;* orcid.org/0000-0001-5365-1120; Email: djn@jila.colorado.edu

Author

David A. Nicholson − *National Institute of Standards and Technology and University of Colorado, JILA, Boulder, Colorado 80309, United States; Department of Chemistry, University of Colorado, Boulder, Colorado 80309, United States*

Complete contact information is available at: https://pubs.acs.org/10.1021/acs.jpcb.1c01036

Notes

The authors declare no competing financial interest.

■ ACKNOWLEDGMENTS

The authors thank Johannes Hohlbein for providing the PDA code. Primary support for this work has been through the National Science Foundation under grant CHE-1665271 from the Chemical, Structure, Dynamics and Mechanisms-A Program, with additional support for development of the confocal/TIRF apparatus from PHY-1734006 (Physics Frontier Center Program). We would also like to acknowledge early seed contributions by the W. M. Keck Foundation Initiative in RNA Sciences at the University of Colorado, Boulder. D.A.N. would like to gratefully acknowledge predoctoral fellowship support from the National Institutes of Health Molecular Biophysics Training Grant (T32 GM-065103).

■ REFERENCES

(1) Alemán, E. A.; Lamichhane, R.; Rueda, D. Exploring RNA folding one molecule at a time. *Curr. Opin. Chem. Biol.* **2008**, *12*, 647−654.

(2) Buchner, G. S.; Murphy, R. D.; Buchete, N.-V.; Kubelka, J. Dynamics of protein folding: Probing the kinetic network of folding-unfolding transitions with experiment and theory. *Biochim. Biophys. Acta, Proteins Proteomics* **2011**, *1814*, 1001−1020.

(3) Grima, R.; Walter, N. G.; Schnell, S. Single-molecule enzymology à la Michaelis-Menten. *FEBS J.* **2014**, *281*, 518−530.

(4) van Oijen, A. M. Single-molecule approaches to characterizing kinetics of biomolecular interactions. *Curr. Opin. Biotechnol.* **2011**, *22*, 75−80.

(5) Stratmann, S. A.; van Oijen, A. M. DNA replication at the single-molecule level. *Chem. Soc. Rev.* **2014**, *43*, 1201−1220.

(6) Friedman, L. J.; Gelles, J. Multi-wavelength single-molecule fluorescence analysis of transcription mechanisms. *Methods* **2015**, *86*, 27−36.

(7) Elf, J.; Barkefors, I. Single-molecule kinetics in living cells. *Annu. Rev. Biochem.* **2019**, *88*, 635−659.

(8) Barkai, E.; Garini, Y.; Metzler, R. Strange kinetics of single molecules in living cells. *Phys. Today* **2012**, *65*, 29−35.

(9) Goryaynov, A.; Ma, J.; Yang, W. Single-molecule studies of nucleocytoplasmic transport: From one dimension to three dimensions. *Integr. Biol.* **2012**, *4*, 10−21.

(10) Guan, J.; Jia, C.; Li, Y.; Liu, Z.; Wang, J.; Yang, Z.; Gu, C.; Su, D.; Houk, K. N.; Zhang, D.; et al. Direct single-molecule dynamic detection of chemical reactions. *Sci. Adv.* **2018**, *4*, No. eaar2177.

(11) Tachikawa, T.; Majima, T. Single-molecule, single-particle approaches for exploring the structure and kinetics of nanocatalysts. *Langmuir* **2012**, *28*, 8933−8943.
(12) Roy, R.; Hohng, S.; Ha, T. A practical guide to single-molecule FRET. *Nat. Methods* **2008**, *5*, 507−516.
(13) Lerner, E.; Cordes, T.; Ingargiola, A.; Alhadid, Y.; Chung, S.; Michalet, X.; Weiss, S. Toward dynamic structural biology: Two decades of single-molecule Foerster resonance energy transfer. *Science* **2018**, *359*, 288.
(14) Sustarsic, M.; Kapanidis, A. N. Taking the ruler to the jungle: Single-molecule FRET for understanding biomolecular structure and dynamics in live cells. *Curr. Opin. Struct. Biol.* **2015**, *34*, 52−59.
(15) Kinz-Thompson, C. D.; Bailey, N. A.; Gonzalez, R. L. Precisely and accurately inferring single-molecule rate constants. *Methods in Enzymology*; Spies, M., Chemla, Y. R., Eds.; Academic Press, 2016; Vol. *581*, pp 187−225.
(16) Bronson, J. E.; Fei, J.; Hofman, J. M.; Gonzalez, R. L., Jr.; Wiggins, C. H. Learning rates and states from biophysical time series: A Bayesian approach to model selection and single-molecule FRET data. *Biophys. J.* **2009**, *97*, 3196−3205.
(17) Hadzic, M. C. A. S.; Börner, R.; König, S. L. B.; Kowerko, D.; Sigel, R. K. O. Reliable state identification and state transition detection in fluorescence intensity-based single-molecule Forster resonance energy-transfer data. *J. Phys. Chem. B* **2018**, *122*, 6134−6147.
(18) Tang, J.; Sun, Y.; Pang, S.; Han, K. Y. Spatially encoded fast single-molecule fluorescence spectroscopy with full field-of-view. *Sci. Rep.* **2017**, *7*, 10945.
(19) Corle, T. R.; Kino, G. S. *Confocal Scanning Optical Microscopy and Related Imaging Systems*; Academic Press: San Diego, 1996.
(20) Tan, Y.-W.; Hanson, J. A.; Chu, J.-W.; Yang, H. Confocal single-molecule FRET for protein conformational dynamics. *Methods Mol. Biol.* **2014**, *1084*, 51−62.
(21) Gopich, I.; Szabo, A. Theory of photon statistics in single-molecule Forster resonance energy transfer. *J. Chem. Phys.* **2005**, *122*, 014707.
(22) Schrangl, L.; Göhring, J.; Schütz, G. J. Kinetic analysis of single molecule FRET transitions without trajectories. *J. Chem. Phys.* **2018**, *148*, 123328.
(23) Santoso, Y.; Torella, J. P.; Kapanidis, A. N. Characterizing single-molecule FRET dynamics with probability distribution analysis. *ChemPhysChem* **2010**, *11*, 2209−2219.
(24) Kalinin, S.; Valeri, A.; Antonik, M.; Felekyan, S.; Seidel, C. A. M. Detection of structural dynamics by FRET: A photon distribution and fluorescence lifetime analysis of systems with multiple states. *J. Phys. Chem. B* **2010**, *114*, 7983−7995.
(25) Chen, J.; Pyle, J. R.; Sy Piecco, K. W.; Kolomeisky, A. B.; Landes, C. F. A two-step method for smFRET data analysis. *J. Phys. Chem. B* **2016**, *120*, 7128−7132.
(26) Elf, J.; Li, G.-W.; Xie, X. S. Probing transcription factor dynamics at the single-molecule level in a living cell. *Science* **2007**, *316*, 1191.
(27) Hansen, A. S.; Woringer, M.; Grimm, J. B.; Lavis, L. D.; Tjian, R.; Darzacq, X. Robust model-based analysis of single-particle tracking experiments with Spot-On. *eLife* **2018**, *7*, No. e33125.
(28) Fontana, M.; Fijen, C.; Lemay, S. G.; Mathwig, K.; Hohlbein, J. High-throughput, non-equilibrium studies of single biomolecules using glass-made nanofluidic devices. *Lab Chip* **2019**, *19*, 79−86.
(29) Farooq, S.; Hohlbein, J. Camera-based single-molecule FRET detection with improved time resolution. *Phys. Chem. Chem. Phys.* **2015**, *17*, 27862−27872.
(30) Gopich, I. V.; Szabo, A. Decoding the pattern of photon colors in single-molecule FRET. *J. Phys. Chem. B* **2009**, *113*, 10965−10973.
(31) Börner, R.; Kowerko, D.; Hadzic, M. C. A. S.; König, S. L. B.; Ritter, M.; Sigel, R. K. O. Simulations of camera-based single-molecule fluorescence experiments. *PLoS One* **2018**, *13*, No. e0195277.
(32) Nicholson, D. A.; Sengupta, A.; Nesbitt, D. J. Chirality-dependent amino acid modulation of RNA folding. *J. Phys. Chem. B* **2020**, *124*, 11561−11572.
(33) Nicholson, D. A.; Sengupta, A.; Sung, H.-L.; Nesbitt, D. J. Amino acid stabilization of nucleic acid secondary structure: Kinetic insights from single-molecule studies. *J. Phys. Chem. B* **2018**, *122*, 9869−9876.
(34) Smith, C. L.; Milea, J. S.; Nguyen, G. H. Immobilization of nucleic acids using biotin-strept(avidin) systems. In *Immobilisation of DNA on Chips II*; Wittmann, C., Ed.; Springer Berlin Heidelberg: Berlin, Heidelberg, 2005, pp 63−90.
(35) Aitken, C. E.; Marshall, R. A.; Puglisi, J. D. An oxygen scavenging system for improvement of dye stability in single-molecule fluorescence experiments. *Biophys. J.* **2008**, *94*, 1826−1835.
(36) Ha, T.; Tinnefeld, P. Photophysics of fluorescent probes for single-molecule biophysics and super-resolution imaging. *Annu. Rev. Phys. Chem.* **2012**, *63*, 595−617.
(37) Axelrod, D.. Total internal reflection fluorescence microscopy. *Methods in Cell Biology*; 1; Elsevier Inc., 2008; Vol. *89*, pp 169−221.
(38) Stigler, J.; Rief, M. Hidden markov analysis of trajectories in single-molecule experiments and the effects of missed events. *ChemPhysChem* **2012**, *13*, 1079−1086.
(39) Blanco, M.; Walter, N. G. Analysis of complex single-molecule FRET time trajectories. *Methods Enzymol.* **2010**, *472*, 153−178.
(40) Al-Mohy, A. H.; Higham, N. J. Improved inverse scaling and squaring algorithms for the matrix logarithm. *SIAM J. Sci. Comput.* **2012**, *34*, C153−C169.
(41) Cheng, S. H.; Higham, N. J.; Kenney, C. S.; Laub, A. J. Approximating the logarithm of a matrix to specified accuracy. *SIAM J. Matrix Anal. Appl.* **2001**, *22*, 1112−1125.
(42) Chodera, J. D.; Noé, F. Markov state models of biomolecular conformational dynamics. *Curr. Opin. Struct. Biol.* **2014**, *25*, 135−144.
(43) Lee, T.-H. Extracting kinetics information from single-molecule fluorescence resonance energy transfer data using hidden markov models. *J. Phys. Chem. B* **2009**, *113*, 11535−11542.
(44) McKinney, S. A.; Joo, C.; Ha, T. Analysis of single-molecule FRET trajectories using hidden Markov modeling. *Biophys. J.* **2006**, *91*, 1941−1951.
(45) Lee, T.-H.; Lapidus, L. J.; Zhao, W.; Travers, K. J.; Herschlag, D.; Chu, S. Measuring the folding transition time of single RNA molecules. *Biophys. J.* **2007**, *92*, 3275−3283.
(46) Lu, H. P. Sizing up single-molecule enzymatic conformational dynamics. *Chem. Soc. Rev.* **2014**, *43*, 1118−1143.
(47) Lerner, E.; Ploetz, E.; Hohlbein, J.; Cordes, T.; Weiss, S. A quantitative theoretical framework for protein-induced fluorescence enhancement-Forster-type resonance energy transfer (PIFE-FRET). *J. Phys. Chem. B* **2016**, *120*, 6401−6410.

https://doi.org/10.1021/acs.jpcb.1c01036
J. Phys. Chem. B 2021, 125, 6080−6089